10ème Congrès Français d'Acoustique
Lyon, 12-16 Avril 2010

Detection of Propeller Noise under Low SNR with the Cyclic Modulation Coherence (CMC)

Jerome Antoni[1], David Hanson[2]

[1]University of Technology of Compiegne, 60205 Compiegne, France, e-mail: antoni@utc.f
[2]Dynamics Group – Sinclair Knight Merz, St Leonards, Sydney, Australia

Underwater detection of the presence of a ship is usually achieved by intercepting the noise radiated by its propeller. In the far-field and in a noisy marine environment, this task is hindered by the rapid decline of the SNR in the frequency band containing the harmonics of the propeller rotation. The traditional approach, largely grounded on empirical observations, consists in demodulating the broadband noise generated by propeller cavitation in the high-frequency end of the spectrum where the SNR is somewhat better preserved. This communication gives a theoretical justification to this methodology by recognizing that high-frequency propeller noise is essentially second-order cyclostationary. Using cyclostationary signal processing offers advantages over existing techniques, in that no user interaction is required to design pass band filters, and superior "cyclic frequency" resolution can be obtained thereby affording more accurate shaft speed estimates and the ability to discriminate multiple propeller shafts operating at slightly different speeds. This paper presents further development of the cyclostationary detection technique, focusing on the definition of statistical thresholds to allow automatic detection of propeller craft based on superior detection metrics. The performance of these thresholds and improved metrics is demonstrated using simulation and measured signals.

1 Introduction

A core function of submarines is the ability to detect surface craft while remaining undetected themselves. A key instrument in this capability is passive sonar, in which the acoustic signals re-corded by the hydrophones on the submarine are processed to recover hidden information. This operation is distinct from the traditional "ping" of active sonar which identifies the presence of the ship from reflected acoustic waves, but in the process alerts the surface ship to the presence and location of the submarine.

One technique for blindly identifying the presence of a ship from hydrophone recordings is DEMON processing, referring to Detection of Envelope Modulation On Noise. As the name suggests, DEMON processing is a form of envelope analysis, where harmonics associated with the shaft speed and blade pass frequencies of a propeller are identified from the envelope spectrum of a filtered signal. The performance of DEMON processing is dependent on the characteristics of the broad-band pass-band filter which is first applied to the data, and is traditionally tuned by an experienced operator to emphasise the modulation in amplitude associated with the propeller rotation.

In this way, DEMON processing seeks to transform a periodicity at the second order, i.e. periodicity in the flow of energy in the signal, into a first order periodicity that manifests as harmonics in a spectrum. It was shown in [1] however, that a far more powerful set of tools is made available by utilising this second order periodicity explicitly; i.e. by recognising that the amplitude modulated pressure signal produced by the propeller is cyclostationary.

In [1], use was made of the Cyclic Modulation Spectrum (CMS) which is a frequency – cyclic frequency (i.e. modulation frequency) spectrum that displays information on the modulation frequency components in the signal explicitly. It was shown that the CMS offered superior resolution in the cyclic frequency domain thereby affording much more accurate estimates of the shaft and blade pass frequencies than traditional envelope analysis (e.g. DEMON processing). Indeed, as explained by Antoni [4], the CMS is analogous to envelope analysis, but whereas envelope analysis seeks to isolate a particular frequency band in order to examine the modulations therein, the CMS analyses every frequency band simultaneously.

One of the recommendations from [1] was the development of statistical thresholds that would ultimately allow the detection process to be performed automatically. This paper presents an advance towards that objective, with the development of statistical thresholds that define a probability of detection as a function of cyclic frequency.

Thresholds for detecting the presence of cyclostationarity in signals have been developed previously for applications in e.g. telecommunications [5] and machine condition monitoring [6]. In [5], Zivanovic and Gardner propose a DCS (Degree of Cyclostationarity) measure based on the distance between the nonstationary autocorrelation and the nearest stationary autocorrelation. For a stationary process, the DCS = 0, whereas for cyclostationary signals, DCS>0. Along similar lines, Raad et al present in [6] an Indicator of Cyclostationarity (ICS) for cyclostationarity of order n = 1-4, which is based on the nth order cumulants in the signal. In this case, at the second order the ICS represents the energy normalised autocovariance of the signal, which for $\alpha>0$ reduces to zero for the null hypothesis that the signal is stationary.

The approach developed in this paper is based on the Cyclic Modulation Coherence, and provides an exact threshold of cyclostationarity as a function of all the computation parameters. It has the advantages that it closely mimics statistical tests based on the cyclic spectral coherence which are optimal in several instances, it is extremely fast to compute, and it applies whenever the

cyclic frequency bandwidth to scan is not greater than about 4 times the frequency resolution Δf, which is a common situation in most sonar applications.

1. Cyclostationary modelling of propeller noise

1.1. Sound field radiated by a statistically equivalent compact source

This section models the propeller noise as originating from a compact source of noise that reproduce similar statistical effects in the far field as observed from experimental data. This approach is quite common for the purpose of noise prediction, the point being not so much to capture the subtle physics of local and complex phenomena that arise around the propeller blades. To start with, the sound field produced by the rotation a single blade is considered only, that resulting from a marine propeller being simply a summation of the former over several blades. Second, the prediction of sound is in the far field, in an unbounded homogenous medium. This implies in particular that wave reflections on the sea surface and bottom will not be accounted for, because not of direct concern for our purpose (although secondary paths could easily be modelled on the basis of the proposed approach). As a result, the problem has an axial symmetry and, without loss of generality, its analysis can be restricted to the horizontal plane intersected by the propeller axis. Third, as is common in propeller noise theory, the action of the propeller blade on a fluid volume is modelled by a moving condensed force $\boldsymbol{F}(t)$ located at a distance r_0 from the hub with a thrust component $F_T(t)$ oriented along the propeller axis and a drag component $F_D(t)$ oriented along the ortho-radial direction -- see Fig.1. The thrust and drag components both contain an DC value that produces the net force of motion and torque, respectively, and an AC value that fluctuates randomly as a function of time that reflects "turbulent loading" of the fluid due to cavitation, inflow turbulence, and various blade edge effects which do not contribute directly to the net force of motion and torque but contribute considerably to the radiated noise. Namely, $F_T(t) = \bar{F}_T + f_T(t)$ and $F_D(t) = \bar{F}_D + f_D(t)$ such that $\bar{F}_T = \langle F_T(t) \rangle$ and $\bar{F}_D = \langle F_D(t) \rangle$ with $\langle \bullet \rangle$ standing for the time average symbol. Cavitation bubbles produced by the rotation of the blade also constitute a major source of noise which is a characteristic feature of the acoustical signature of surface ships. It is conveniently modelled as an equivalent rotating monopole concentrated at $\boldsymbol{r}_0$ with an effective point source strength $Q(t)$. As before, let $Q(t) = \bar{Q} + q(t)$ where $\bar{Q}$ and $q(t)$ are DC and stationary randomly fluctuating components, respectively. Fourth, the propeller blade is assumed to rotate with constant speed Ω, so that its current position is $\theta = \Omega t$ with $\theta = 0$ along the x axis -- see Fig.1. The rotation takes place in a spatially non-uniform flow owing to circumferential variation in the wake field and to the vertical gradient of the hydrostatic pressure. This is modelled, in a first approach, by multiplying the moving force $\boldsymbol{F}(t)$ by some periodic function $w_2(\theta) = w_2(\theta + \Omega)$ and the point source strength $Q(t)$ by $w_1(\theta) = w_1(\theta + \Omega)$.

Fifth, the underwater ambient noise is modelled by adding a stationary random process $\nu(t)$ on the measurement returned by the hydrophone at the observer location. As is usually the case, the power spectral density of the ocean background noise is assumed to decrease as a function of frequency. The assumption of stationarity is obviously simplistic, but without direct implication as explained later in the paper.

Under these assumptions, the sound field produced at time t at the observation position $\boldsymbol{r}_1$ by the moving point force $w(\theta)\boldsymbol{F}(t)$ at position $\boldsymbol{r}_0$ is [1]

$$p(\boldsymbol{r}_1, t) = \left[\frac{(\boldsymbol{r}_1 - \boldsymbol{r}_0)}{4\pi c_0 r^2 (1 - M_r)^2} \cdot \left(\frac{\partial w_2(\theta)\boldsymbol{F}(t)}{\partial t} + \frac{w_2(\theta)\boldsymbol{F}(t)}{1 - M_r} \frac{\partial M_r}{\partial t} \right) \right] \frac{1}{4\pi} \frac{\partial}{\partial t} \left[\frac{w_1(\theta) Q(t)}{r} \right] + \nu(t) \tag{1}$$

where c_0 is the speed of sound in the medium, $r = |\boldsymbol{r}_1 - \boldsymbol{r}_0|$ is the distance from the observer to the moving force, $M_r = \left(\boldsymbol{r} \cdot \partial \boldsymbol{r}_0 / \partial t\right) / r c_0$ is the Mach number in the direction of the observer, and where the square brackets $[\bullet]$ around the whole expression indicates that the latter is to be evaluated at the retarded time $\tau = t - r/c_0$.

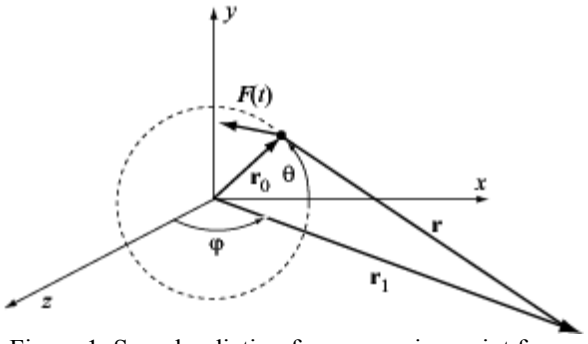

Figure 1: Sound radiation from a moving point force representing the action of a propeller blade on the fluid medium

1.2. Tonal and broadband noise in the far field

After some calculations and simplifications relating to the far-field assumption, Eq. (1) shows that the overall radiated noise comprises a tonal part

$$p_{\text{tonal}}(\boldsymbol{r}_1, t) = [g_1(\theta) w_2(\theta) \Omega \left(\dot{w}_2(\theta) \left(\bar{F}_T \cos\varphi - \bar{F}_D \sin\theta \sin\varphi \right) - g_2(\theta) \left(\bar{F}_T M \cos\varphi + \bar{F}_D \right) \right) + g_3(\theta) \dot{w}_1(\theta) \bar{Q} \tag{2}$$

with $M = \Omega r_0 / c_0$ the rotational Mach number, φ the angle of observation with the z axis, $g_1(\theta) = 1/4\pi c_0 r_1 (1 + M \sin\theta \sin\varphi)^2$, $g_2(\theta) = \left(r_0/r_1 - \sin\varphi\cos\theta\right)/(1 + M \sin\theta \sin\varphi)$, and $g_2(\theta) = (1 + M \sin\theta \sin\varphi)/4\pi r_1$, which radiates energy at multiples of the rotation speed Ω. As for the broadband part, it comes

$$p_{\text{broadband}}(\boldsymbol{r}_1,t) = g_1(\theta)\dot{w}(\theta)\Omega\left(f_T(t)\cos\varphi - f_D(t)\sin\theta\sin\varphi\right) + w(\theta)g_1(\theta)\left(\dot{f}_T(t)\cos\varphi - \dot{f}_D(t)\sin\theta\sin\varphi\right) - \Omega g_2(\theta)\left(f_T(t)M\cos\varphi + f_D(t)\right) + g_3(\theta)w_1(\theta)\dot{q}(t) \quad (3)$$

which radiates energy over a continuum of frequencies. The extent of the tonal noise spectrum is typically limited to a few harmonics when the modulating functions $g_1(\theta)w(\theta)$, $g_2(\theta)$ and $g_3(\theta)\dot{w}_1(\theta)$ are smooth, whereas the broadband noise spectrum covers a much wider range of frequencies due to cavitation noise and its amplification in high frequencies by the time derivative appearing in the second term of the left-hand-side of Eq. (3) -- experimental spectra of cavitation noise show a "white noise" behaviour that extents far beyond the audible range [3].

As a last consequence of Eqs. (2) and (3), it is seen that the amplitude of both tonal and broadband noise dramatically decreases like $1/r$ in the far field. Since tonal noise typically occupies the same frequency band as underwater ambient noise, the signal-to-noise decreases to so small a level when it arrives at the hydrophone that its detection by classical spectral analysis is no longer feasible. Broadband noise, on the other hand, has its energy spread high enough in frequency to maintain a good signal-to-noise ratio against low-frequency ambient noise even in the far-field. This explains why the spectrum of propeller noise, as measured in the far field, may turn out completely broadband, without any remaining discrete frequency component, somehow in contradiction with the intuition that tonal noise radiates more efficiently than broadband noise.

1.3. Broadband noise is cyclostationary

The previous section has given some insights into the reasons why the sound radiated in the far field by a marine propeller emerges from the ambient background noise as broadband noise, thus explaining why measured spectra actually look "continuous". However, broadband noise still contains the information on hidden periodicities in the form of periodic modulations due to the Doppler effect and the rotation of blades in a non-uniform flow. Equation (3) is explicit in this regard. First, it involves a periodic amplitude modulation through multiplication by $\sin\theta$, $g_1(\theta)$, and $g_2(\theta)$, $w(\theta)$ and $\dot{w}(\theta)$. Second, its evaluation at the retarded time $\tau \approx t - r_1/c_0 + (r_0/c_0)\cos\theta\sin\varphi$ introduces a periodic phase modulation. These are two reasons why the radiated broadband noise is actually not stationary, but nonstationary with periodic modulations, that is cyclostationary. Cyclostationarity is the mechanism by which a broadband (high-frequency) wave can carry a discrete (low-pass) information.

2 The cyclic modulation coherence

The cyclic modulation coherence (CMC) is a power-normalised version of the cyclic modulation spectrum recently introduced in [4]. The CMC intends to approximate the cyclic spectral coherence while offering a much faster way of computation by making a systematic use of the discrete Fourier transform (DFT) and its related FFT algorithm.

Let $\{x(n)\}$, $n = 0,\ldots,L\text{-}1$ be the L-long discrete signal to be analysed. A N-long analysis window $w(n)$ – typically a Hanning window – is introduced and shifted along the signal by steps of R samples, such that $x(n)w_i(n)$ -- with $w_i(n) = w(n\text{-}iR)$ -- smoothly cuts off a block of the signal around time samples $n = iR,\ldots,iR+N\text{-}1$. Note that there are $I = [L/R]$ such overlapping blocks in the signal, with 1 - R/N the fraction of overlap. The next step is to compute the DFT

$$X_N(t_i,f) = \sum_{n=iR}^{iR+N-1} x(n)w_i(n)e^{-j2\pi nf} \quad (4)$$

which is a function of time $t_i = iR$ and of frequency f – the so-called short-time Fourier trans-form (STFT). As explained before, this is not enough to detect a cyclostationary signal which, in general, is not periodic in its waveform but allows a random carrier to transmit energy with periodic bursts in some frequency band. The detection of such a behaviour is achieved by means of a second DFT on the squared-magnitude of $X_N(t_i,f)$ that transforms time t_i into its dual frequency variable α:

$$P_x(\alpha,f) = \frac{1}{I}\sum_{i=0}^{I-1} |X_N(t_i,f)|^2 \, e^{-j2\pi\alpha t_i} \quad (5)$$

The quantity $P_x(\alpha,f)$ was coined the cyclic modulation spectrum in [4] because of its ability to detect periodic modulation of random noise. In short, it is simply the DFT of the so-called spectrogram $|X_N(t_i,f)|2$. Note that, in the special case where $\alpha = 0$, $P_x(0,f)$ boils down to the averaged-periodogram estimate of the power spectral density $S_x(f)$ (PSD) of the signal. The CMC is then defined as

$$CMC(\alpha,f) = \frac{P_x(\alpha,f)}{P_x(0,f)} \quad (6)$$

that is the cyclic modulation spectrum normalised by the estimated PSD so as to eliminate all scaling effects. Therefore the capability of detecting the presence of cyclostationarity in some frequency band will not depend on the actual level energy in that band, but only whether energy fluctuates therein periodically or not. Note that the normalisation is also equivalent to computing the cyclic modulation spectrum of the whitened signal, which is a customary preprocessing step in most detection tests.

3 Detection of cyclostationarity

In order to understand the behaviour of the CMC in the presence of cyclostationarity -- and in particular how it relates to the cyclic spectral coherence -- let us investigate its expression in the simple case where signal $x(n)$ exhibits cyclostationarity at a single and arbitrary cyclic frequency α_0 (note this is without loss of generality, since the result will be duplicated accordingly in the case of multiple cyclic frequencies). In that case, according to the definition of cyclostationarity, one looks for the presence a sinusoidal component in the squared-magnitude STFT, i.e.

$$|X_N(t_i,f)|^2 = A_0(f)\cos(2\pi\alpha_0 t_i + \varphi_0) + |N_N(t_i,f)|^2 \quad (7)$$

where $A_0 > 0$, φ_0 is an arbitrary phase, and $|N_N(t_i,f)|^2$ a stationary "noise" component that contains a high enough DC level such that $|X_N(t_i,f)|^2 \geq 0$. Under some mild assumptions about the smoothness of the PSD of $x(n)$, it can be shown that

$$CMC(\alpha, f) = D_I(R\alpha) + \frac{A_0(f)}{2S_x(f)} D_I(R\alpha - R\alpha_0) \quad (8)$$

where

i) the Dirichlet kernel, $D_I(R\alpha) = e^{-j\pi\alpha R(I-1)} \boldsymbol{K}^{-1} \sin(\pi\alpha RI)/\sin(\pi\alpha R)$ is the only function of α and therefore controls the cyclic frequency resolution, i.e. $\Delta\alpha \approx 1/IR \approx 1/L$ as returned by the width of its main lobe,

ii) the "cyclostationary" signal-to-noise ratio (SNR) $0 \leq A_0(f)/2S_x(f) \leq 1$ returns the strength of the cyclostationary component relatively to the signal power at frequency f,

Therefore, because $D_I(R\alpha)$ rapidly tends to a train of discrete delta functions with period 1/R,

$$CMC(\alpha, f) \underset{I}{\rightarrow} \begin{cases} 1, & \alpha = 0 \\ \dfrac{A_0(f)}{2S_x(f)}, & \alpha_0 + p/R, \text{ for any interger } p \\ 0, & \text{elsewhere.} \end{cases} \quad (9)$$

This is fine enough to detect the presence cyclostationarity at $\alpha = \alpha_0$, but not fully satisfying since the CMC also returns non-zero values at all other cyclic frequencies $\alpha = \alpha_0 + p/R$, thus erroneously indicating other cyclostationary components where there are not. The reason stems from undersampling the STFT by factor R in Eq.(4) which entails frequency aliasing in α. In order to gain more insight into this issue and see how to solve it, it must be realised that $A_0(f)$ in Eq. (7) is obtained as

$$\frac{A_0}{2} = \kappa_w(\alpha_0) S_x(\alpha_0, f) \quad (10)$$

where $\kappa_w(\alpha) = R_w(\alpha_0)/R_w(0)$ with $R_w(\alpha) = \sum_{n=0}^{N-1} w(n)^2 e^{-j2\pi\alpha n}$ and where $S_x(f,\alpha_0)$ is the cyclic power spectrum defined as in [8]

$$S_x(f, \alpha_0) = \lim_{N\to\infty} \lim_{I\to\infty} \frac{1}{I \cdot R_w(0)} X_N(t_i, f) X_N^*(t_i, f - \alpha_0) \quad (11)$$

with * the complex conjugate symbol. In Eq. (10), $\kappa_w(\alpha_0)$ is seen to act as a low-pass filter in α which gradually brings down $A_0(f)$ to zero as α_0 increases. For instance, for a N-long Hanning window, $\kappa_w(0) = 1$ and $\kappa_w(|\alpha_0| \geq \alpha_{max}) \approx 0$ with $\alpha_{max} \approx 4/N$. The reason for this becomes clear if one construes the STFT $X_N(t_i,f)$ as a narrow band-pass filtered signal in band $[f-\Delta f/2, f+\Delta f/2]$ where $\Delta f \sim 1/N$. Hence, the narrower the band, the slower the variations of the energy flow $|X_N(t_i,f)|^2$ through it, with cut-off frequency $|\alpha| \leq \alpha_{max} \approx 4\Delta f$, meaning that the narrower the band, the slower the variations of the energy flow $|X_N(t_i,f)|^2$ through it – beyond intuition, this may also be proved as a direct consequence of the uncertainty principle [4]. The existence of such a cut-off frequency is actually a chance to reject the undesirable aliased cyclic frequencies $\alpha = \alpha_0 + p/R$, $|p| > 1$ in Eq. (9). This is achieved provided that $1/R > \alpha_{max}$, i.e. $R \leq N/4$ with a Hanning window, meaning that at least 75% overlap should be set when computing the STFT in Eq. (4). The CMC is then non-zero at $\alpha = 0$ and $\alpha = \alpha_0$ only, thus detecting cyclostationarity at the correct location.

A final remark concerns the magnitude of the CMC at the cyclic frequency α_0 which, according to Eqs. (9) and (10), is asymptotically

$$CMC(\alpha_0, f) \underset{I}{\rightarrow} \frac{A_0(f)}{2S_x(f)} = \kappa_w(\alpha_0) \frac{S_x(\alpha_0, f)}{S_x(f)} \quad (12)$$

Being proportional to the ratio $S_x(f,\alpha_0)/S_x(f)$, this is a measure of the degree of cyclostationarity of the signal. Indeed, if α_0 is smaller than the variations of $S_x(f)$ – which is consistent with the previous assumption $|\alpha_0| \leq 4\Delta f$ -- then $S_x(f,\alpha_0)/S_x(f) \approx \gamma_x(f,\alpha_0)$, the cyclic spectral coherence, a quantity which returns a measure of cyclostationarity within 0 and 1. The magnitude of the CMC is also found proportional to $\kappa_w(\alpha_0)$ which, as explained above, places a limit α_{max} beyond which the CMC virtually vanishes. This is the most serious drawback of the CMC as compared to the cyclic spectral coherence which does not suffer from such a limitation. Figure 2 illustrates the main features of the CMC discussed in this paragraph.

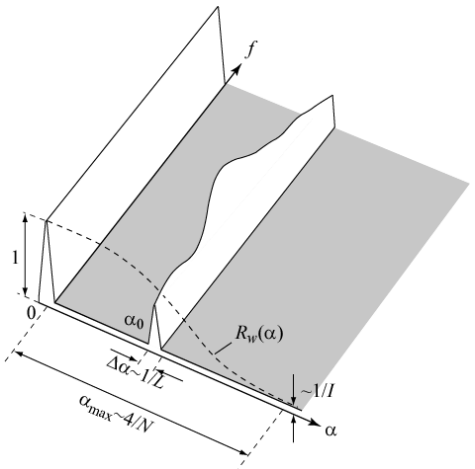

Figure 2: Schematic illustration of the CMC in the presence of cyclostationarity at cyclic frequency α_0. The length L of the signal controls the cyclic frequency resolution $\Delta\alpha \approx 1/IR \approx 1/L$ and the length N of the analysis window the cyclic frequency bandwidth $\alpha_{max} \approx 4/N$. The shaded area indicates regions of theoretical zero values but affected by estimation noise.

4 Statistical test

The CMC was demonstrated to correctly detect the presence of cyclostationarity in a limited cyclic frequency range. In most sonar applications this will be fine enough, since the cyclic frequency of interest will usually be much smaller that the coarser allowable spectral resolution, i.e. $|\alpha_0| < \Delta f$, which is consistent with the previous

requirement that $|\alpha_0| < \alpha_{max}$ with $\alpha_{max} \leq 4/N$. Moreover, the CMC being a complex quantity in general, its squared-magnitude will be used as far as detection is of concern. The image formed by $|CMC(\alpha,f)|^2$ as a function of α and f will then provide a good and fast *visual test* to check for the presence of cyclostationarity in the signal. Once a frequency band $[f1,f2]$ is identified where cyclostationarity is present, a better *statistical test* is then given by the integrated squared-magnitude CMC (ICMC), namely,

Reject the null hypothesis H0 "there is no presence of cyclostationarity at cyclic frequency α_0 (i.e. $A_0(f) = 0$)" at the p level of significance if :

$$\frac{1}{K}\sum_{k=k1}^{k2} |CMC(\alpha_0, f_k)|^2 > \lambda_{1-p}(\alpha_0) \qquad (13)$$

where $K = k_1 - k_2$ with k_1 and k_2 the DFT bins corresponding to f_1 and f_2 and $\lambda_{1-p}(\alpha_0)$ a statistical threshold to be determined. By allowing the user to select a relevant frequency band where the cyclostationary SNR is high, the proposed statistical test will be all the more efficient. In addition, because of the integration over frequency f, the test will amount to comparing a function of α only against the threshold $\lambda_{1-p}(\alpha)$. It now remains to find the level of that threshold in the general case, as a function of the number K of integrated frequency bins, the number I of signal blocks, the shift R between adjacent blocks, the length N and the type of the analysis window $w(n)$.

4.1 Statistical threshold under the null hypothesis

The statistical threshold $\lambda_{1-p}(\alpha)$ reflects that level the ICMC should not exceed with a risk probability p when the signal is assumed stationary at cyclic frequency α. Stated differently, it should envelop 100(1-p)% of the values of the squared-magnitude estimation noise $|N_M(t_i,f)|^2$ in Eq. (7). It may be found as follows. First, it is noticed that as a consequence of the Central Limit theorem applied to the DFT [7] under the null hypothesis, the CMC is asymptotically complex Gaussian with zero mean and variance

$$\sigma^2(\alpha) = \frac{1}{RI}\sum_{m=0}^{N-1} R_w(m)^2 \cos(2\pi\alpha m) \qquad (14)$$

Equation (14) gives the expression of the baseline embodied by $|N_M(t_i,f)|^2$ in Eq. (7) – see Fig. 4. The normalised squared-magnitude CMC is then distributed as $\sigma^2(\alpha)/2 \cdot \chi_2^2$, where χ_2^2 is a Chi2 variable with 2 degrees of freedom. Since the frequency bins of the DFT are asymptotically independent under H0 [7], the sum of K Chi2 variables with 2 degrees of freedom then follows another Chi2 variable with 2K degrees of freedom. Hence,

$$\frac{1}{K}\sum_{k=k1}^{k2} |CMC(\alpha, f_k)|^2 \overset{d}{\approx} \frac{\sigma^2(\alpha)}{2K}\chi_{2K}^2 \qquad (15)$$

Based on this result, the statistical threshold is finally found as $\lambda_{1-p}(\alpha) = \chi_{1-p,2K}^2 \cdot \sigma^2(\alpha)/(2K)$ with $\chi_{1-p,2K}^2$ the 100(1-p)th percentile of the χ_{2K}^2 distribution.

5. Results

The application of the statistical thresholds described above is demonstrated here with an example. This simulation considers four signals, each of length 32768 samples with sampling frequency 10kHz; a) a stationary signal, b) a cyclostationary signal with α_0 =20 Hz and SNR = -10dB, c) a cyclostationary signal with α_0 =20 Hz and SNR = 0dB, and d) a cyclostationary signal with α_0 =70 Hz and SNR = 0dB.

The CMC of each of these signals is shown in Fig. 3, where the effect of the low-pass filter $R_w(\alpha)$ on α_0 =70 Hz is particularly evident. The integrated CMC of each of these signals is shown in Fig. 4 where the detection performance in case (b) is particularly noteworthy considering the very low SNR in this case.

The detection strategy described above was also applied to measured data of a North Sea Coaster, as shown in Fig. 5, again with excellent results.

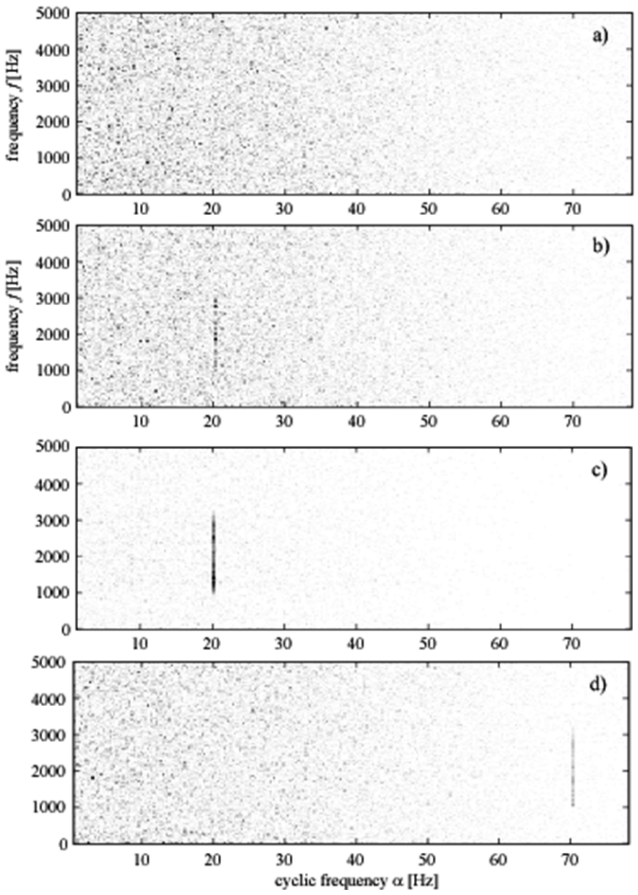

Figure 3: cyclic modulation coherence in the case of a) a stationary signal, b) a cyclostationary signal with α_0 =20 Hz and SNR = -10dB, c) a cyclostationary signal with α_0 =20 Hz and SNR = 0dB and d) a cyclostationary signal with α_0 =70 Hz and SNR = 0dB. ($\Delta\alpha$ = 0.3Hz and Δf = 39Hz.)

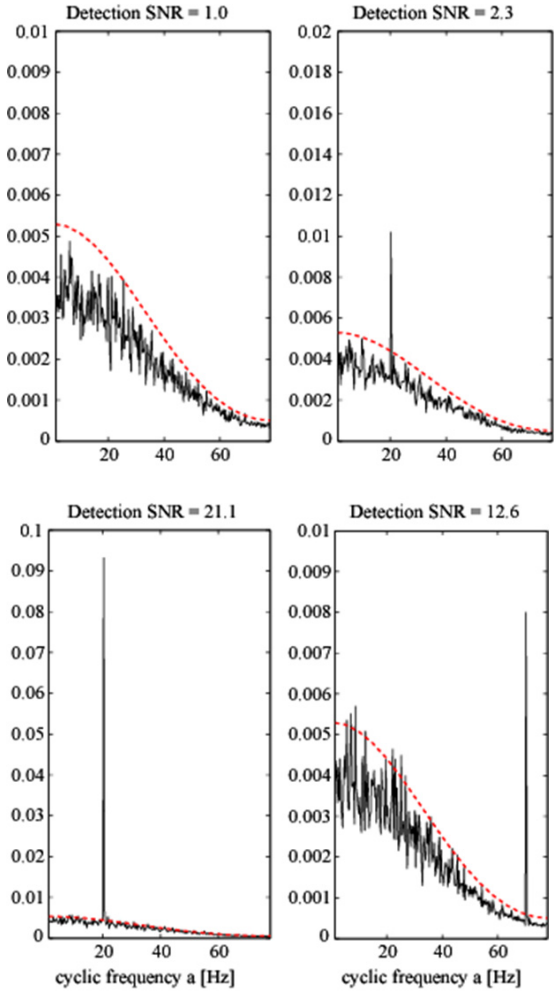

Figure 4: integrated squared-magnitude cyclic modulation coherence in the band [1000,3000]Hz in the four cases of Fig. 3 together the statistical threshold (red dotted line) at the 0,5% level of significance.

6. Conclusions and Further Work

This paper presented a new method for detecting propeller craft from sonar signals, i.e. identifying second order cyclostationary signals in significant extraneous noise. The method is based on the Cyclic Modulation Coherence and provides a statistical threshold, based on a probability of detection, for cyclostationarity in a signal as a function of cyclic frequency. The technique was demonstrated on both simulated and measured signals and provides, at this stage, a visual aid for sonar operators to assist in detecting surface ships.

It is ultimately envisaged that the statistical threshold will be incorporated into a cyclostationary detection and identification framework which will include not only automatic detection (through further development of the work presented in this paper), but also array processing to determine range, speed and heading, and narrow-band cyclic spectral analysis to try and identify specific properties of individual classes of ship.

Références

[1] Hanson, D, J. Antoni, G. Brown, R. Emslie, "Cyclostationarity for Passive Underwater Detection of Propeller Craft: A Development of DEMON Processing", *Proceedings of Acoustics 2008*, 24-26 November 2008, Geelong, Australia

[2] Lowson M. V., "The sound field for singularities in motion", Proc. of the The Royal Societey of London. Series A, Mathematical and Physical Sciences, Volume 286, Issue 1407, pp. 559-572 (1965).

[3] Marine propellers and propulsion, John Carlton, Butterworth-Heinemann; 2 edition (2007)

[4] Antoni, J, "Cyclostationarity by Examples", *Mechanical Systems and Signal Processing*, Vol 23, Issue 4, 987-1036 (2009).

[5] Zivanovic, G. and W. Gardner, "Degrees of cyclostationarity and their application to signal detection and estimation", *Signal Processing*, 22, 287-297 (1991).

[6] Raad, A., J. Antoni, M. Sidahmed, "Indicators of cyclostationarity: Theory and application to gear fault monitoring", *Mechanical Systems and Signal Processing*, 22, 574–587 (2008).

[7] Brillinger, David R. "Time series: data analysis and theory", *SIAM*, 2001

[8] Gardner, W.A., "On the Spectral Coherence of Nonstationary Processes", *IEEE Transactions on Signal Processing*, Volume 39, Issue 2, 424 - 430 (1991).

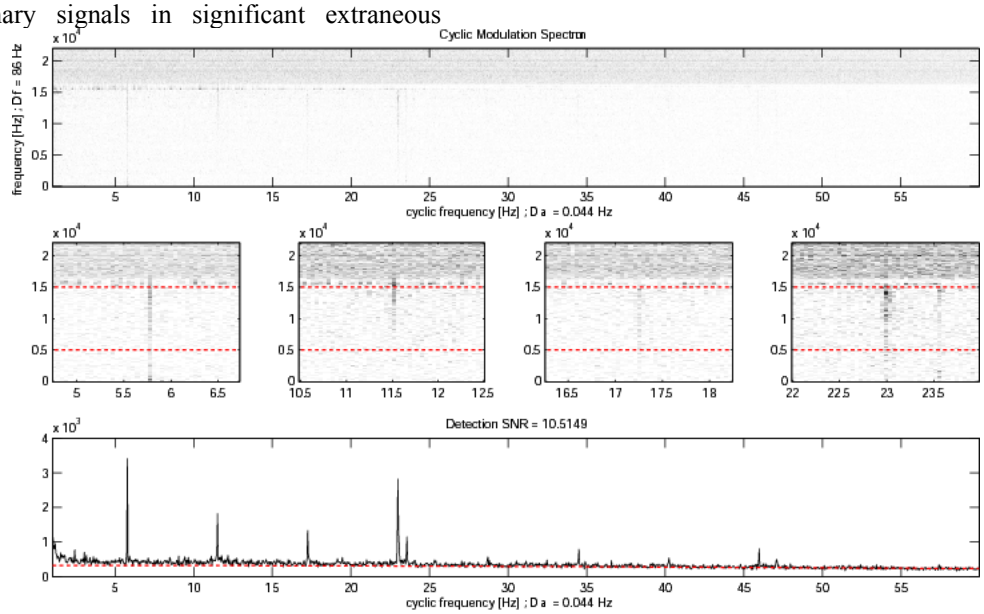

Figure 5 Cyclostationary detection of a North Sea Coaster; CMS (top), CMS at harmonics of shaft speed showing frequency range for integration (middle) and integrated CMS (bottom) with threshold